FATIGUE CRACK RETARDATION MODELS BASED ON MECHANISMS ACTING BEHIND, AT OR AHEAD OF THE CRACK TIP[1]

Jaime Tupiassú Pinho de Castro[2]
Marco Antonio Meggiolaro[2]
Antonio Carlos de Oliveira Miranda[3]

Abstract
The classes of mechanisms that can cause load sequence effects on fatigue crack growth are divided into mechanisms that act *behind*, *at* or *ahead* of the crack tip. After reviewing the crack closure idea, a mechanism which acts *behind* the crack tip, and presenting crack tip bifurcation (which acts *at* the crack tip), quantitative models to predict the effects *ahead* the crack tip due to damage accumulation are proposed and verified. In these models, fatigue cracking is assumed caused by the sequential failure of volume elements or tiny εN specimens in front of the crack tip, calculated by damage accumulation concepts. The crack is treated as a sharp notch with a small but not zero radius, avoiding the physically unrealistic singularity at its tip. In this way, the damage caused by each load cycle, including the effects of residual stresses, can be calculated at each element ahead of the crack tip using the correct hysteresis loops caused by the loading. The presented approaches are extended to predict fatigue crack growth under variable amplitude loading. The damage accumulation model is evaluated assuming that the width of the volume element broken at each cycle is equal to the region ahead of the crack tip that suffers damage beyond its critical value. The quite reasonable predictions of the measured fatigue crack growth behavior in steel specimens under service loads validate the discussed models.
Key words: Fatigue crack retardation; Closure; Bifurcation; Critical damage; Residual stresses.

MODELOS DE RETARDO DE TRINCAS DE FADIGA BASEADOS EM MECANISMOS QUE ATUAM ANTES, NA OU À FRENTE DA PONTA DA TRINCA

Resumo
Os tipos de mecanismos que podem causar retardos no crescimento das trincas de fadiga são divididos em mechanisms que atuam *antes*, *na* ou *à frente* da ponta da trinca. Depois de rever a idéia do fechamento da trinca, que atua *antes* de sua ponta, e de apresentar a bifurcação (que atua *na* ponta da trinca), modelos quantitativos para quantificar o dano acumulado *à frente* da ponta da trinca são propostos e verificados. Nestes modelos, supõe-se que o trincamento por fadiga é causado pela falha seqüencial de elementos de volume, ou minúsculos espécimens εN, à frente da ponta da trinca, devido ao dano que eles acumulam durante a história da carga. A trinca é tratada como um entalhe afiado com uma ponta de raio muito pequeno, mas não zero, para evitar a singularidade na ponta da trinca, que não é fisicamente realista. Desta forma, o dano causado por cada evento da carga, incluindo os efeitos das tensões residuais, pode ser calculado em cada elemento de volume à frente da ponta da trinca, usando os laços de histerese corretos causados pela carga. Este método é em seguida generalizado para considerar cargas de amplitude variável, supondo que o elemento de volume que falha à frente da ponta da trinca tem a largura (variável) da região onde o dano acumulado é maior que o crítico. Por fim resultados experimentais que confirmam a validade desta modelagem são apresentados e discutidos.
Palavras-chave: Retardo de trincas de fadiga; Fechamento; Bifurcação; Dano crítico; Tensões residuais.

[1] *Technical Contribution to the 61st International Congress of the ABM, January 24-27th 2006, Rio de Janeiro – RJ – Brazil.*
[2] *Mechanical Engineer, Ph.D., Professor Dept. Mechanical Eng., PUC-Rio*
[3] *Civil Engineer, Ph.D., Tecgraf, PUC-Rio*

1 INTRODUCTION

There are many mechanisms that can retard or accelerate the growth of a fatigue crack after significant load amplitude variations.[1-2] Moreover, these mechanisms generally can act simultaneously, with their relative importance in any problem depending on several factors such as crack and piece sizes, dominant stress state at the crack tip, microstructure of the material, mean load, and environment. These load interaction mechanisms can act ***behind***, ***at*** or ***ahead*** of the crack tip, e.g.:

- crack closure (***behind*** the crack tip), which can be caused by plasticity, oxidation or roughness of the crack faces, or even by strain induced phase transformation, e.g.,
- crack tip blunting, kinking or bifurcation (***at*** or close to the crack tip), and
- residual stress and strain fields (***ahead*** of the crack tip).

Most models of load sequence effects in fatigue crack growth (FCG) are still based on the Elberian plasticity-induced crack closure. But there are several problems that cannot be explained by the effective stress intensity range ΔK_{eff} concept. E.g. a strong objection (3) against crack closure is based on convincing experimental evidence such as fatigue crack growth threshold values ΔK_{th} that are higher in vacuum than in air. Another problem that cannot be explained by crack closure is crack delays or arrests under high $R = K_{min}/K_{max}$ ratios, when the minimum value K_{min} of the applied range $\Delta K = K_{max} - K_{min}$ always remains *above* K_{op}, the (measured) load that opens the fatigue crack.[4-5]

2 OVERLOAD-INDUCED BIFURCATION AS A MECHANISM ACTING AT THE CRACK TIP

Crack tip blunting is not an efficient retardation mechanism (because K_t, the stress concentration factor of a blunt fatigue crack, is always very high), but overload-induced crack bifurcation can be. Mixed-mode conditions acting near to the tip of a bifurcated crack (even when the far-field stress is pure traction) can retard or even arrest the subsequent fatigue crack growth behavior because the equivalent SIF K_b and K_c of the longer and shorter branches can be considerably smaller than that of a straight crack with the same projected length. Moreover, very small differences between the branch lengths **b** and **c** are enough to cause the shorter branch **c** to arrest as the longer one **b** keeps propagating, in the general case changing its curvature and retarding its growth rate until reaching approximately its pre-OL SIF and growth direction and rate.

Some analytical solutions have been obtained for the SIF of kinked and branched cracks, but it is very difficult to develop complete analytical solutions to describe their complex propagation behavior. Thus, numerical methods are usually the only practical means to predict the propagation behavior of branched cracks. A summary of such SIF solutions is presented in Suresh and Shih.[6]

The **Quebra** FE code is an ideal tool to predict the (generally curved) path of a branched crack and to calculate the associated Modes I and II SIF. Its very efficient meshing algorithm is fundamental to avoid elements with poor aspect ratio, since the ratio between the size scale of the larger and smaller elements can be above 1,000 in crack bifurcation calculations. The calculated K_b and K_c can be exported to the **ViDa** general-purpose fatigue life prediction code, where using any appropriate fatigue crack propagation rule the retardation effects can be modeled. Such method predicted within a factor of two the overload-induced retadation in several experiments, as discussed in Miranda et al.[7] and Majumdar and Morrow.[8]

3 A NON-SINGULAR RETARDATION MODEL ACTING AFTER THE CRACK TIP

The damage *ahead* of a fatigue crack tip can be estimated supposing that fatigue cracks grow by sequentially breaking small volume elements (VE) ahead of their tips, which fracture when the crack tip reaches them *because* they accumulated all the damage the material can support. Then, **εN** procedures can be combined with fracture mechanics concepts to predict FCG. These models can consider the VE width in the FCG direction as being the distance that the crack grows on each cycle, or the FCG rate as being the VE width divided by the number of cycles that the crack would need to cross it. Critical damage models are not new,[9-15] but still need improvements. Most models assume a singular stress/strain field ahead of the crack tip (concentrating in this way all the damage next to the tip) and need some adjustable constant to fit the FCG data, compromising their prediction potential. But the supposed singularity at the crack tip is a characteristic of the mathematical models that postulate a zero radius tip, not of the real cracks, which have a blunt tip when loaded (and finite strains at their tip, or else they would be unstable).

To avoid this problem, the actual finite strain range at the crack tip $\Delta\varepsilon_{tip}$ can be estimated using the stress concentration factor $\mathbf{K_t}$ for the blunt crack[16] and a strain concentration rule. The strain range field ahead of the crack tip can then be upper-bounded by $\Delta\varepsilon_{tip}$ (e.g. by assuming $\Delta\varepsilon_{tip}$ constant where the singular solution would predict strains greater than $\Delta\varepsilon_{tip}$). Supposing that all fatigue damage occurs inside this region next to the tip, the number of cycles $\mathbf{N^*}$ associated with $\Delta\varepsilon_{tip}$ can be obtained from Coffin-Manson's rule, and the FCG rate as the length of this region divided by $\mathbf{N^*}$. But such models have two shortcomings. First, neglecting the fatigue damage elsewhere concentrates it in the very last $\mathbf{N^*}$ cycles, a non-conservative hypothesis. Second, assuming an intermittent and not a cycle-by-cycle FCG is certainly not true for most metallic structures (althout it may be true for some polymers).

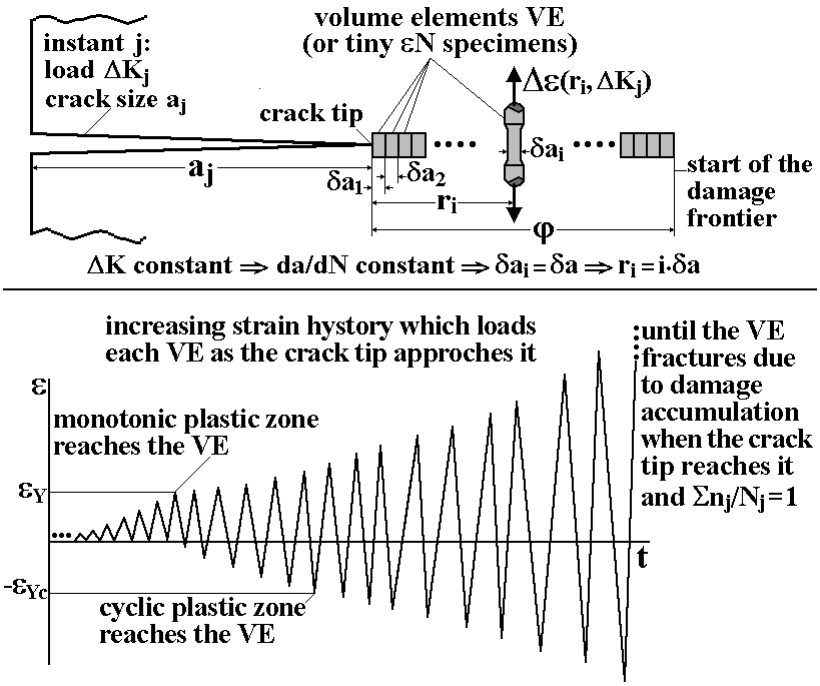

Figure 1. Schematics of the FCG assumed to be caused by the sequential fracture of volume elements (or tiny **εN** specimens) at every load cycle.

To avoid these limitations, the model proposed here[5,13-15] removes the crack tip singularity by shifting the origin of the strain field from the crack tip to a point inside the crack, located by matching the tip strain with $\Delta\varepsilon_{tip}$ predicted by a strain concentration rule,

such as Neuber,[17] Molsky and Glinka,[18] or the linear rule.[19] This approach recognizes that the strain range $\Delta\varepsilon(r, \Delta K)$ in an unbroken VE increases and causes damage in each load cycle as the crack tip approaches it, see Figure 1. Therefore, the VE closest to the tip breaks due to damage accumulation during all the previous load cycles.

This model is then extended to deal with the VA loading case, recognizing that the VE that breaks in any given cycle has *variable* width, which should be calculated by locating the point ahead of the crack tip where the accumulated damage reaches a specified value (e.g. 1.0 when using Miner's rule). Load sequence effects, such as overload-induced crack growth retardation, are associated with hysteresis loop shifts and with mean load effects on the material εN curve, and can be calculated using the powerful numerical tools available in the **ViDa** software.[20] Moreover, this model can recognize an opening load, and thus can separate the cyclic damage from the closure contributions to the crack growth process.

4 CONSTANT AMPLITUDE LOADING

In every load cycle, each VE ahead of the crack tip suffers strain hysteresis loops of increasing range as the tip approaches it, and suffers a damage increment that depends on its distance from the tip and on the load ΔK_j at that event. The fracture of a VE near the crack tip occurs when its accumulated damage reaches a critical value, e.g. $\Sigma n_j/N_j = 1$ by Miner's rule, where n_j is the number of cycles of the **j**-th load event and N_j is the number of cycles that the piece would last if loaded solely by that event. If under constant ΔK (or ΔK_{eff}) the fatigue crack advances a fixed distance δa in every load cycle, and if the damage outside the cyclic plastic zone zp_c is neglected, there are $zp_c/\delta a$ VE ahead of the crack tip at any instant. As zp_c advances with the crack, each new load cycle breaks the VE adjacent to the crack tip, induces an increased strain range in all other unbroken VE, and adds a new element to the damage zone. Thus, as each load cycle causes a growth increment, $n_j = 1$. Moreover, since the VE are considered as small εN specimens, they break when:

$$\sum_{i=0}^{zp_c/\delta a} \frac{1}{N(zp_c - i\cdot\delta a)} = \sum_{r_i=0}^{zp_c} \frac{1}{N(r_i)} = 1 \qquad (1)$$

where $N(r_i) = N(zp_c - i\cdot\delta a)$ is the life corresponding to the plastic strain range $\Delta\varepsilon_p(r_i)$ acting at a distance r_i from the crack tip, calculated using Coffin-Manson's rule,

$$\Delta\varepsilon_p(r_i) = \frac{2S_{Yc}}{E}\cdot\left(\frac{zp_c}{r_i}\right)^{\frac{1}{1+h_c}} \qquad (2)$$

and $\Delta\varepsilon_p(r_i)$ in its turn can be described by Schwalbe's[10] modification of the HRR field:

$$N(r_i) = \frac{1}{2}\left(\frac{\Delta\varepsilon_p(r_i)}{2\varepsilon_c}\right)^{1/c} \qquad (3)$$

where S_{Yc} is the cyclic yield strength, h_c is the cyclic hardening exponent, and zp_c is the cyclic plastic zone in plane strain, estimated, e.g., by Duran et al.[14] (ν is Poisson's coefficient):

$$zp_c = \frac{(1-2\nu)^2}{4\pi\cdot(1+h_c)}\cdot\left(\frac{\Delta K}{S_{Yc}}\right)^2 \Rightarrow \quad N(r_i) = \frac{1}{2}\left[\frac{S_{Yc}}{E\varepsilon_c}\cdot\left(\frac{zp_c}{r_i}\right)^{\frac{1}{1+h_c}}\right]^{1/c} \qquad (4)$$

The HRR field assumes an idealized crack tip, thus it is singular at $r = 0$. But no infinite strain are physically admissible (which does not mean that singular models are useless, only that the damage close to the crack tip is not predictable by them). To avoide this

unrealistic strain singularity, the origin of the HRR coordinate system is shifted into the crack by a small distance **X**, following Creager and Paris.[16] Approximating the VE width **δa** by a differential **da** at a distance **dr** ahead of the crack tip and the Miner's summation by an integral, which is easier to deal with:

$$\Delta\varepsilon_p(r+X)=\frac{2S_{Yc}}{E}\cdot\left(\frac{zp_c}{r+X}\right)^{\frac{1}{1+h_c}} \tag{5}$$

$$\frac{da}{dN}=\int_0^{zp_c}\frac{dr}{N(r+X)} \tag{6}$$

To determine **X** and **N(r + X)** two paths can be followed. The first uses Creager and Paris' **X = ρ/2**, ρ being the actual crack tip radius, estimated by **ρ = CTOD/2**:

$$X=\frac{\rho}{2}=\frac{CTOD}{4}=\frac{K_{max}^2\cdot(1-2\nu)}{\pi\cdot E\cdot S_{Yc}}\cdot\sqrt{\frac{1}{2(1+h_c)}} \tag{7}$$

The second, instead of arbitrating the strain field origin offset, first determines **X** by calculating the crack (linear elastic) stress concentration factor K_t:[16]

$$K_t=2\Delta K/(\Delta\sigma_n\cdot\sqrt{\pi\rho}) \tag{8}$$

For any given **ΔK** and **R** it is possible to calculate ρ and K_t from Miranda et al.[7] and Majumdar and Morrow.[8]

Using a cyclic strain hardening coefficient H_c and exponent h_c in Ramberg-Osgood and negleting the elastic strain range, the Linear, Neuber and Molsky and Glinka concentration rules predictions for $\Delta\varepsilon_{tip}$ at the crack tip are, respectively:

$$\Delta\varepsilon_{tip}=\frac{K_t\cdot\Delta\sigma_n}{E}=\frac{2\Delta K}{E\sqrt{\pi\cdot CTOD/2}} \tag{9}$$

$$\begin{cases}\Delta\sigma_{tip}\cdot\Delta\varepsilon_{tip}=\cdot\dfrac{(K_t\Delta\sigma_n)^2}{E}=\dfrac{8\Delta K^2}{E\cdot\pi\cdot CTOD}\\ \Delta\varepsilon_{tip}=2\left(\dfrac{\Delta\sigma_{tip}}{2H_c}\right)^{1/h_c}\end{cases} \tag{10}$$

$$\begin{cases}\dfrac{2\Delta K^2}{E\cdot\pi\cdot CTOD}=\dfrac{\Delta\sigma_{tip}^2}{4E}+\dfrac{\Delta\sigma_{tip}}{1+h_c}\cdot\left(\dfrac{\Delta\sigma_{tip}}{2H_c}\right)^{1/h_c}\\ \Delta\varepsilon_{tip}=2\left(\dfrac{\Delta\sigma_{tip}}{2H_c}\right)^{1/h_c}\end{cases} \tag{11}$$

After calculating $\Delta\varepsilon_{tip}$ using one of these rules, the shift **X** of the HRR origin is obtained by:

$$\Delta\varepsilon_{tip}=\frac{2S_{Yc}}{E}\cdot\left(\frac{zp_c}{X}\right)^{\frac{1}{1+h_c}}\Rightarrow X=zp_c\cdot\left(\frac{2S_{Yc}}{E\Delta\varepsilon_{tip}}\right)^{1+h_c} \tag{12}$$

The strain distribution at a distance **r** ahead of the crack tip, $\Delta\varepsilon_p$**(r + X)**, without the singularity problem at the crack tip, can now be readily obtained by:

$$\frac{da}{dN}=\int_0^{zp_c}2\cdot\left(\frac{2\varepsilon_c}{\Delta\varepsilon_p(r+X)}\right)^{1/c}dr \tag{13}$$

This prediction was experimentally verified in SAE1020 and API 5L X-60 steels and in a 7075 T6 Al alloy, using (13) to obtain the constant of a McEvily-type **da/dN** equation, which uses only one adjustable parameter:

$$\frac{da}{dN} = A[\Delta K - \Delta K_{th}(R)]^2 \left(\frac{K_c}{K_c - [\Delta K/(1-R)]}\right) \quad (14)$$

where K_c and $\Delta K_{th}(R)$ are the material fracture toughness and crack propagation threshold at the load ratio **R**. To guarantee the consistence of this experimental verification, K_c, $\Delta K_{th}(R)$, the **εN** and the **da/dN** data were all obtained by testing proper specimens manufactured from the same stock of the 3 materials, following ASTM standards. The API 5L X-60 **da/dN**×**ΔK** experimental curves is compared with this simple model predictions in Figure 2 (see (5) for the other curves). Both the shape and the magnitude of the data are quite reasonably reproduced by this model, with the Linear rule generating better predictions probably because the tests were made under predominantly plane-ε conditions. Since no adjustable constant was used in this modeling, it can be concluded that this performance is no coincidence.

But some remarks are required. First, damage beyond zp_c was neglected to simplify the numerical calculations, but as it accumulates at all points ahead of the crack tip, it is wiser to choose the damage origin by numerically testing its influence on **da/dN**, or better by comparing the predictions with FCG tests, as done later on. Second, FE calculations[21] indicate that there is a region adjacent to the blunt crack tip with a strain gradient much lower than predicted by the HRR field. These problems can be avoided by shifting the origin *away* from the tip by x_2 and assuming the crack-tip strain range $\Delta\varepsilon_{tip}$ constant over the region I of length x_1+x_2 shown in Figure 3. x_1 can be obtained equating $\Delta\varepsilon_{tip}$ and the HRR-calculated strain range, and the crack-tip stress range $\Delta\varepsilon_{tip}$ from:

$$\Delta\sigma_{tip} = \Delta\sigma(r = x_1) = 2S_{Yc} \cdot \left(\frac{zp_c}{x_1}\right)^{\frac{h_c}{1+h_c}} = 2S_{Yc} \cdot \left(\frac{E \cdot \Delta\varepsilon_{tip}}{2S_{Yc}}\right)^{h_c} \quad (15)$$

Then, following Irwin's classical idea, the value of the shift x_2 is obtained by integrating the stress field **σ(r)**:

$$\int_0^{\infty} \Delta\sigma(r)dr = \int_0^{x_1+x_2} \Delta\sigma_{tip}dr + \int_{x_1}^{\infty} \Delta\sigma(r)dr \Rightarrow \int_0^{x_1} \Delta\sigma(r)dr = \int_0^{x_1+x_2} \Delta\sigma_{tip}dr \quad (16)$$

Since $x_1 < zp_c$, **Δσ(r)** in the above integral can be described by the HRR solution:

$$\int_0^{x_1} 2S_{Yc} \cdot \left(\frac{zp_c}{r}\right)^{\frac{h_c}{1+h_c}} dr = \Delta\sigma_{tip} \cdot x_1 \cdot (1+h_c) = \Delta\sigma_{tip} \cdot (x_1+x_2) \Rightarrow x_2 = x_1 \cdot h_c \quad (17)$$

These simple tricks generate a more reasonable strain distribution model (Figure 3):

$$\Delta\varepsilon(r) = \Delta\varepsilon_{tip}\ ,\ 0 \le r \le x_1 + x_2 \text{ (region I)} \quad (18)$$

$$\Delta\varepsilon(r) = \frac{2S_{Yc}}{E} \cdot \left(\frac{zp_c}{r-x_2}\right)^{\frac{1}{1+h_c}}\ ,\ x_1 + x_2 < r \le zp_c + x_2 \text{ (region II, shifted HRR)} \quad (19)$$

$$\Delta\varepsilon(r) \cong \frac{2S_{Yc}}{E} \cdot \sqrt{\frac{zp_c+x_2}{r}} \cdot \left(1+\nu\frac{r-zp_c}{zp-zp_c}\right)\ ,\ zp_c + x_2 < r < zp \text{ (region III, interpolation)} \quad (20)$$

$$\Delta\varepsilon(r) = \frac{\Delta K \cdot (1+\nu)}{\kappa E\sqrt{2\pi(r - zp/2)}}\ ,\ r \ge zp \text{ (region IV, shifted Irwin)} \quad (21)$$

where $\kappa = 1$ for plane stress and $\kappa = (1-2\nu)$ for plane strain, and

$$zp = \frac{1}{\pi\kappa^2} \cdot \left(\frac{K_{max}}{S_{Yc}}\right)^2 \text{ and } zp_c = \frac{1}{4\pi\kappa^2 \cdot (1+h_c)} \cdot \left(\frac{\Delta K}{S_{Yc}}\right)^2 \quad (22)$$

Both CA and VA FCG can then be calculated using equations (18-22) which consider all the damage ahead of the crack tip and provide a more realistic model of the FCG

process. But (2), (5) and (13) must be modified to include elastic parameters σ_c and **b**, and to account for the mean load σ_m effects on the VE life using Morrow elastic, Morrow elastic-plastic or Smith-Topper-Watson equations. But the life **N** in these equations cannot be explicitly written as a function of the VE strain range and mean load and thus must be calculated numerically, a programming task that is far from trivial.

5 VARIABLE AMPLITUDE LOADING

The **da/dN**×**ΔK** curve predicted for CA can be used with some load interaction engineering model in the **ViDa** software for VA problems. But the idea here is to *directly* quantify the fatigue damage induced by the VA load considering the crack growth as caused by the sequential fracture of *variable* size VE ahead of the crack tip. Since the Linear strain concentration rule generated better predictions above, it is the only one used here, and as load interaction effects can have a significant importance in FCG, they are modeled by using Morrow elastic equation to describe the VE fatigue life:

$$N(r+X)=\frac{1}{2}\left(\frac{\Delta\varepsilon_p(r+X)}{2\varepsilon_c}\left(1-\frac{\sigma_m}{\sigma_c}\right)^{-c/b}\right)^{1/c} \tag{23}$$

To account for mean load effects, a modified stress intensity range can be easily implemented for **R > 0** to filter the loading cycles that cause no damage by using:

$$\Delta K_{eff} = K_{max} - K_{PR} = \frac{\Delta K}{1-R} - K_{PR} \tag{24}$$

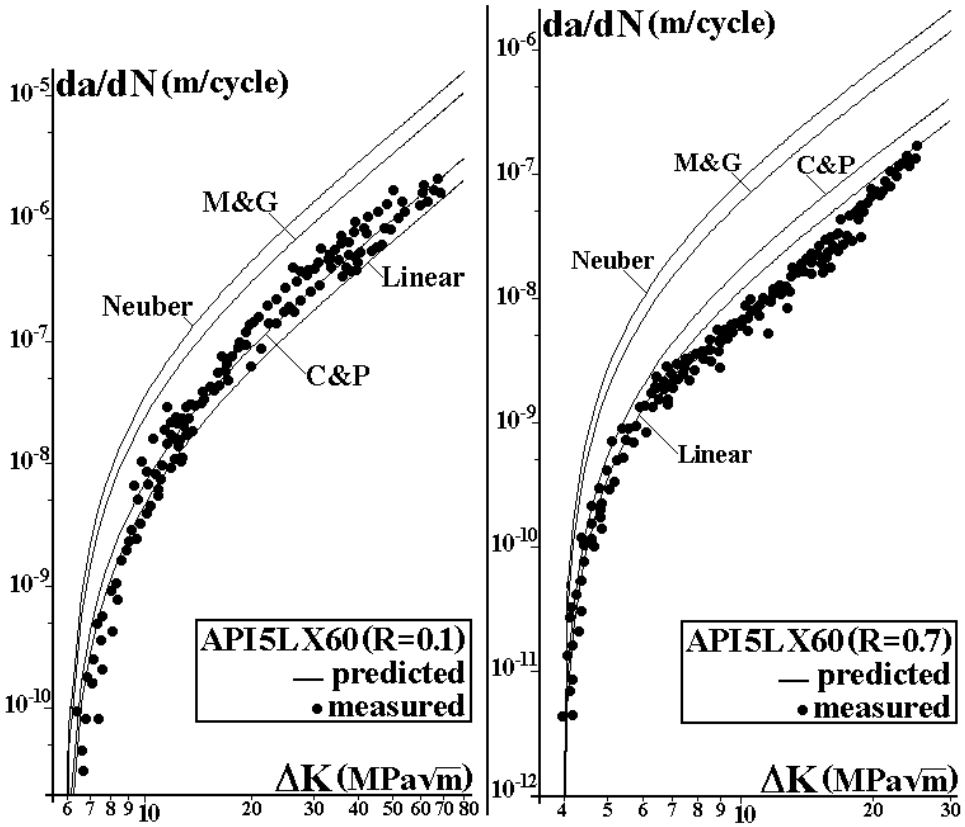

Figure 2. da/dN×ΔK measured and ***predicted*** by various strain concentration rules used in the critical damage model, for API-5L-X60 steel at **R = 0.1** and **R = 0.7**.

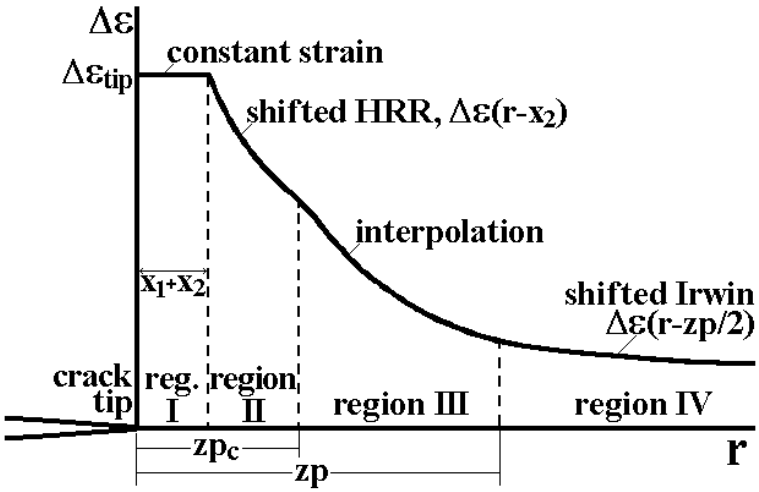

Figure 3. Proposed strain range distribution, divided in 4 regions to consider both the elastic and the plastic contributions to the damage ahead of the crack tip.

where K_{PR} is a propagation threshold that depends on the considered retardation mechanism, such as K_{op} or K_{max}^{*} from the Unified Approach (3). The damage function for each cycle is then:

$$d_i\left(r+X_i\right)=\frac{n_i}{N_i\left(r+X_i\right)} \tag{25}$$

If the material ahead of the crack is supposed virgin, then its increment δa_1 caused by the first load event is the value $r = r_1$ that makes Equation (25) equal to one, therefore:

$$d_1\left(r_1+X_1\right)=1 \quad \Rightarrow \quad \delta a_1=r_1 \tag{26}$$

In all subsequent events, the crack increments take into account the damage accumulated by the previous loading, in the same way it was done for the constant loading case. But as the coordinate system moves with the crack, a coordinate transformation of the damage functions is necessary:

$$D_i=\sum_{j=1}^{i} d_j\left(r+\sum_{p=j}^{i-1}\delta a_p\right) \tag{27}$$

Since the distance $r = r_i$ where the accumulated damage equals one in the **i**-th event is a variable that depends on ΔK_i (or ΔK_{eff_i}) and on the previous loading history, VE of different widths may be broken at the crack tip by this model. This idea is illustrated by the events schematized in Figure 4.

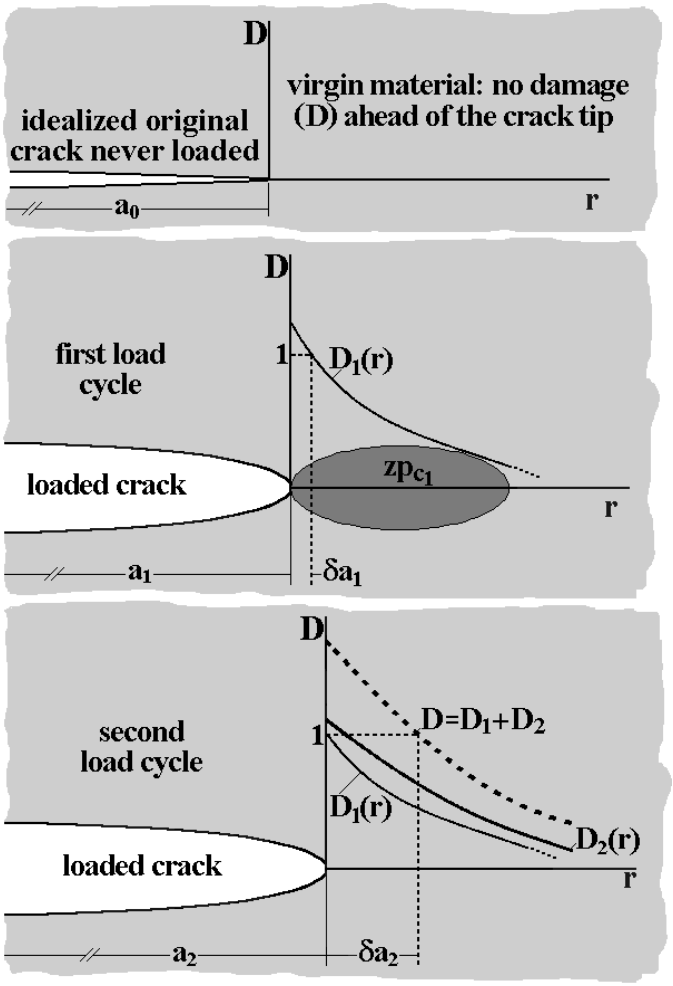

Figure 4. Schematics of the critical damage calculations, which under variable amplitude loading recognize variable crack increments by forcing the crack to grow over the region where **D = 1**.

6 RESULTS AND DISCUSSIONS

FCG tests under VA loading were performed on API-5L-X52 steel **50×10mm** C(T) specimens, pre-cracked under CA at $\Delta K = 20MPa\sqrt{m}$ until reaching crack sizes $a \cong 12.6mm$. These cracks were measured within **20μm** accuracy by optical methods and by a strain gage bonded at the back face of the C(T). The basic monotonic and cyclic properties, measured in computer-controlled servo-hydraulic machines using standard ASTM testing procedures, are $E = 200000$, $S_U = 527$, $S_Y = 430$, $S_{Yc} = 370$, $H_c = 840$, and $\sigma_c = 720$ (all in MPa), $h_c = 0.132$, $\varepsilon_c = 0.31$, $b = -0.076$ and $c = -0.53$. About 50 specimens were tested under deformation ratios varying from $R = -1$ to $R = 0.8$ (at least 2 at each strain range) to obtain the **εN** curve, see Figure 5. Morrow's strain-life equation (23), which includes the mean stress effect only in Coffin-Manson's elastic term, best fit the experimental data. The basic **da/dN** curve, measured using the same equipment, is fitted by $da/dN(R = 0.1) = 2 \cdot 10^{-10}(\Delta K - 8)^{2.4}$ (in **m/cycle**), where $\Delta K_{th}(R = 0.1) = 8MPa\sqrt{m}$.

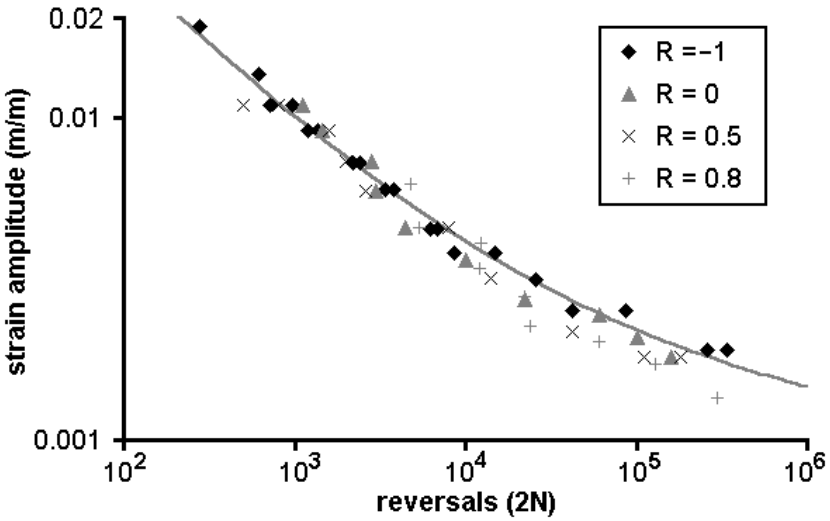

Figure 5. API 5L X52 steel measured strain-life data, and Morrow elastic model that best fitted this data.

FCG tests were then conducted under several VA histories. The history shown in Figure 6 has 50,000 blocks containing 100 reversals each. The high mean stress levels were chosen to avoid crack closure effects. The load history was counted by the sequential rain-flow method, using the **ViDa** software.[20] The damage calculation was made using a specially developed code following all the procedures discussed above. The crack growth predictions based solely on **εN** parameters are again quite reasonable, see Figure 7. The prediction assuming no damage outside the cyclic plastic zone $\mathbf{zp_c}$ underestimated the crack growth. However, when the small (but not insignificant) damage in the material between the cyclic and monotonic plastic zone borders is also included in the calculations, an even better agreement is obtained. Note also that crack growth is slightly underestimated after $1.8 \cdot 10^6$ cycles, probably due to having neglected the elastic damage and the (small) mean stress effects.

A similar test was conducted on AISI 1020 steel, with measured properties $\mathbf{E = 205GPa}$, $\mathbf{S_U = 491}$, $\mathbf{S_Y = 285}$, $\mathbf{S_{Yc} = 270}$, $\mathbf{H_c = 941}$ and $\mathbf{\sigma_c = 815MPa}$, $\mathbf{h_c = 0.18}$, $\mathbf{\varepsilon_c = 0.25}$, $\mathbf{b = -0.114}$, and $\mathbf{c = -0.54}$. The FCG curve fit is $\mathbf{da/dN = 5 \cdot 10^{-10}(\Delta K - \Delta K_{th})^2\{K_c/(K_c - \Delta K/(1 - R))\}}$, where $\mathbf{\Delta K_{th} = 11.6}$ and $\mathbf{K_c = 277}$ (ΔK, ΔK_{th} and K_c in $\mathbf{MPa\sqrt{m}}$ and **da/dN** in **m/cycle**). The VA load history is a series of blocks containing 101 peaks and valleys, as shown in Figure 8, with a duration of two seconds each. Figure 9 compares the predictions with the measured data. This other prediction of fatigue crack growth under VA based only on **εN** properties turns out to be again quite accurate. Therefore, these tests indicate that the ideas behind the proposed critical damage model make sense and deserve to be better explored.

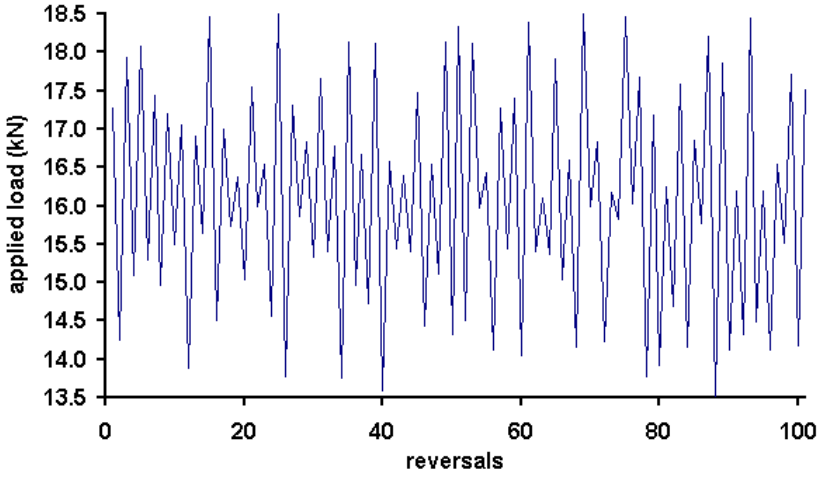

Figure 6. Variable amplitude load block applied to the API-5L-X52 steel C(T). Note the high mean **R**-ratio.

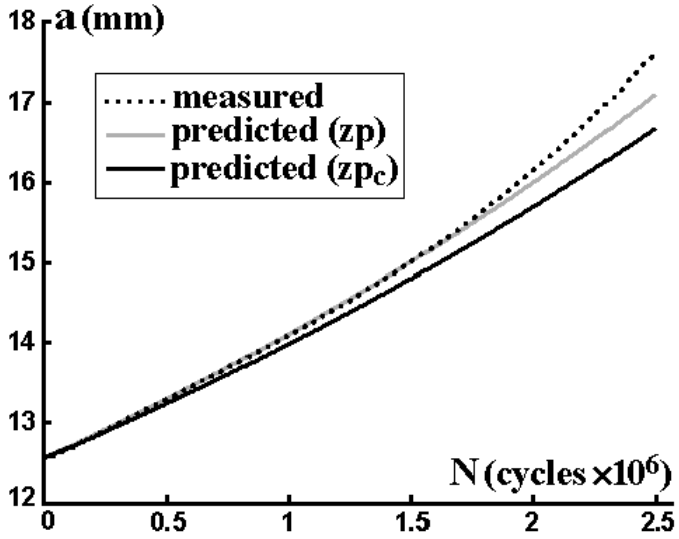

Figure 7. Comparison between the crack growth measurements and the **εN**-based predictions for the variable amplitude load presented in Figure 6 (API-5L-X52 steel).

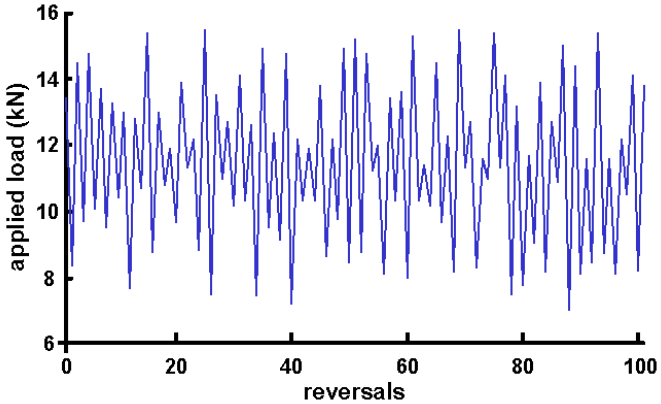

Figure 8. VA load block applied to the SAE 1020 steel C(T). Again a high mean **R**-ratio was used in this test, to avoid the interference of possible significant closure effects which could mask the model performance.

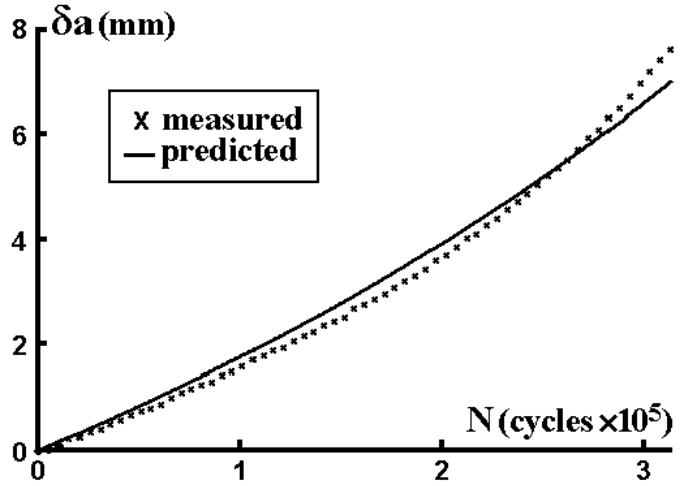

Figure 9. Comparison between the crack growth measurements and the **εN**-based predictions for the variable amplitude load presented in Figure 8 (SAE 1020 steel).

7 CONCLUSIONS

Several mechanisms can cause load sequence effects on fatigue crack growth, and they may act *before*, *at* or *after* the crack tip. Plasticity-induced crack closure is the most popular of them, but it cannot explain sequence effects in various important problems. A damage accumulation model ahead of the crack tip based on **εN** cyclic properties, which can explain those effects in the absence of closure, was proposed for predicting fatigue crack propagation under variable amplitude loading. The model treats the crack as a sharp notch with a small but finite radius to avoid singularity problems, and calculates damage accumulation explicitly at each load cycle. Experimental results show a good agreement between measured crack growth both under constant and variable amplitude loading and the predictions based purely on **εN** data.

REFERENCES

1 SKORUPA,M; *FFEMS* v.21, p.987, 1998
2 SKORUPA,M; *FFEMS* v.22, p.905, 1999
3 SADANANDA,K; VASUDEVAN,AK; HOLTZ,RL; *I. J. Fatigue* v.23, p.S277, 1999
4 MEGGIOLARO,MA; CASTRO,JTP; *I. J. Fatigue* v.25, p.843, 2003
5 CASTRO,JTP; MEGGIOLARO,MA; MIRANDA,ACO; *I. J. Fatigue* v.27, p.1366, 2005
6 SURESH,S; SHIH,CF; *I. J. Fracture* v.30, p.237, 1986
7 MEGGIOLARO,MA; MIRANDA,ACO; CASTRO,JTP; MARTHA,LF; *Eng. Fracture Mechanics* v.72, p.2647, 2005
8 MIRANDA,ACO; MEGGIOLARO,MA; CASTRO,JTP; MARTHA,LF; *I.J. Fatigue* v.27, p.1398, 2005
9 MAJUMDAR,S; MORROW,J; *ASTM STP 559*, p.159, 1974
10 SCHWALBE,KH; *Eng. Fracture Mechanics* v.6, p.325, 1974
11 GLINKA,G; *I. J. Fatigue* v.4, p.59, 1982
12 GLINKA,G; *Eng. Fracture Mechanics* v.21, p.245, 1985
13 CASTRO,JTP; KENEDI,PP; *J. Brazilian Society of Mechanical Sciences* v.17, p.292, 1995
14 DURÁN,JAR; CASTRO,JTP; PAYÃO FILHO,JC; *FFEMS* v.26, p.137, 2003
15 DURÁN,JAR; CASTRO,JTP; MEGGIOLARO,MA; *Fatigue 2002*, p.2759, Blom,AF ed., Emas, 2002
16 CREAGER,M; PARIS,PC; *I. J. Fracture Mechanics* v.3, p.247, 1967
17 NEUBER,H; *J. Applied Mechanics* v.28, p.544, 1961
18 MOLSKY,K; GLINKA,G; *Materials Science and Engineering* v.50, p.93, 1981
19 STEPHENS,R; FATEMI,A; STEPHENS,RR; FUCHS,HO; *Metal Fatigue in Engineering*, Interscience 2000
20 www.tecgraf.puc-rio.br/vida
21 McMeeking,RM; Parks,DM; *ASTM STP 668*, p.175-194, 1979